A Low-Power/Low-Voltage CMOS Wireless Interface at 5.7 GHz With Dry Electrodes for Cognitive Networks

Nuno Sérgio Dias, *Member, IEEE*, João Paulo Carmo, *Member, IEEE*, Paulo Mateus Mendes, *Member, IEEE*, and José Higino Correia, *Member, IEEE*

Abstract—This paper describes a low-power/low-voltage CMOS wireless interface (CMOS-WiI) at 5.7 GHz with dry electrodes for congnitive networks. The electrodes are 4 × 4 microtip arrays and acquire electroencephalogram (EEG) signals in key- points for processing. The CMOS-WiI was fabricated in a UMC 0.18 μm RF CMOS process and its total power consumption is 23 mW with a voltage-supply of only 1.5 V. The carrier frequency is digitally selectable and it can be one of 16 possible values in the range 5.42–5.83 GHz, with 27.12 MHz steps. These multiple carriers allow a better spectrum allocation as well as the acquisition, processing and transmission of high-quality EEG signals from 16 electrode arrays. The microtips array was fabricated through bulk micromachining of a $\langle 100 \rangle$-type silicon substrate in a potassium hydroxide solution and avoids long subject preparations for EEG data acquisition. The reactive sputtering of iridium dioxide (IrO) on the surface of the array guarantees its biocompatibility. The fabrication process was trimmed in a way that each microtip presents solid angles of 54.7°, a width in the range 150–200 μm, a height of 100–200 μm, and a microtip interspacing of 2 μm. The microtips array coated with IrO together with the CMOS-WiI permit the remote monitoring of EEG signals from freely-moving subjects.

Index Terms—Sensor interface, wireless microsystems, wireless sensors networks.

I. INTRODUCTION

THE wireless monitoring of human-body information is an emerging field with an increased importance in bioengineering and rehabilitation [1]. In this context and in contrary to classic approaches (see Fig. 1), new solutions based on wireless EEG modules fit the clinical requirements for ease of placement and removal of the electrodes in a braincap. An electrode (microtips array), microelectronic circuitry (the CMOS-WiI) and an associated antenna are mounted together in a compact wireless EEG module. The power supply of this module is obtained locally from a coin-sized battery placed in the braincap. The operation frequency of 5.7 GHz was selected because it allows the integration of chip size antennas in wireless Microsystems. Moreover, these antennas reduce the impedance mismatches prob-
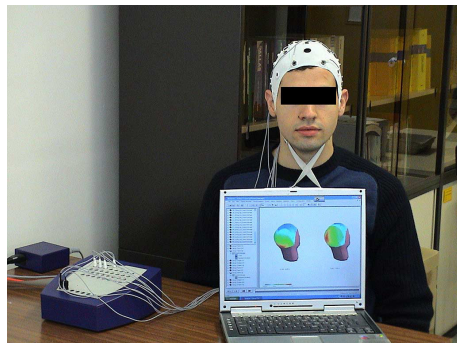
lems, systematize the manufacturing processes, and leads to Microsystems with an even reduced price [2]. The amplification, filtering, and high-resolution digital conversion circuitry are integrated in these small-size individual wireless EEG modules. This solution also enables quick electrode placement or takeoff. The optimization of the number of wireless modules through machine learning techniques enables the monitorization of scalp key-points.

II. STATE-OF-THE ART AND SYSTEM OVERVIEW

Recent advances in the biomedical field related to medicine and biology have demanded more sophisticated electrode fabrication technologies [3]. Electrical activity occurs between neurons as well as in the muscles (e.g., heart) and nerves. The biopotential electrodes, jointly with acquisition systems, sense that electrical activity and make it accessible either for clinical or research trials. Biopotential recording and excitable tissue stimulation have been accomplished by recurring to invasive and non-invasive electrodes.

It has been stated that skin impedance is determined mainly by the *stratum corneum* at frequencies below 10 KHz [4] (see Fig. 2). Furthermore, the EEG applications fall entirely into this frequency range. This outer skin layer has high-impedance characteristics since it is mainly constituted by dead skin cells and has very low water content. Consequently, biopotential electrodes require skin preparation (e.g., skin abrasion) and the use of electrolytic gel to bypass the *stratum corneum* isolation prop-

Fig. 1. Photograph showing a patient using a classic EEG braincap with Ag/AgCl electrodes and respective wires.
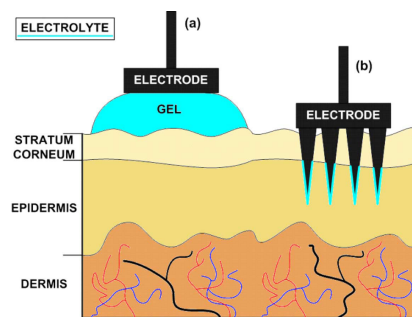

Fig. 2. Application of biopotential electrodes: (a) standard EEG electrode; (b) EEG electrode with microtips.
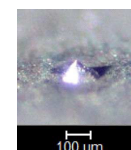

Fig. 3. Magnified photograph of a microtip with pyramidal shape.

erties and reduce interface impedance [Fig. 2(a)]. The electrical activity occurs between neurons as well as in muscles, thus the microtips (that compose the dry electrode) can penetrate through the *stratum corneum* (which is 10 μm thick) and can enter in a closer contact with the biological fluids in the lower layers of the epidermis [Fig. 2(b)]. This avoids the isolating characteristics of the *stratum corneum* and allows the electrodes placement without the need of any conductive gel. However, the length of the microtips cannot exceed the 200 μm, in order to not enter in contact with the sensory receptors and with the nerve endings in the dermis (which is rich in some chlorides like NaCl). The Ag/AgCl has been proposed as a dry electrode coating with promising results [5]. However, the silver chloride proved to be toxic and has an associated infection risk since it dissolves on skin [6]. EEG electrodes made of sputtered iridium oxide (IrO) present better electrochemical properties with low toxicity, when compared with those made of Ag/AgCl [7].

The microtip arrays were coated with IrO by DC-sputtering, after their bulk micromachining through a wet etching process with undercut in a KOH solution, and are at least 100 μm high (see Fig. 3) in order to be able to pass through the outer skin layer (i.e., *stratum corneum*). These features make these electrodes especially suitable for wireless sensors networks, where it is desirable to place wireless modules (with electrodes) on the individual's scalp without the need of conductive gel or skin abrasion.

The selection of the suitable wireless technology plays an important role in ensuring the success of an application in the longterm. In this context, the growth in the demand for using the emerging and established technologies, such as the ZigBee

and the Bluetooth to put connect the different sensors, controllers, and actuators is notable [8]–[10]. These two standards have theirs strong points and drawbacks. The ZigBee is a set of protocols (e.g., corresponding to the two lowest layers in the OSI model) that allows us to mount a real wireless sensor network in topologies ranging from a simple star to complex meshes with the advantage to work for years. This working mode is obtained at the cost to have the wireless nodes to operate in low-duty-cycles. Low-duty-cycles are not tolerable in real-time systems, so the advantage of the ZigBee will fast turns in something to avoid. Alternatively, the Bluetooth allows the use of high-baud rates, e.g., baud rates up to 1 Mbps to exchange data between the wireless nodes. However, it is very difficult to have complex mesh topologies and worse, the Bluetooth is a very heavy protocol with a lot of rules, where despite the high-baud rates available, it will result in high latencies. High latencies are also unacceptable in real-time monitoring and control systems. Thus, the Bluetooth is more suitable in point-to-point applications, such as those used to connect personal computers or hands-free systems (in cars) to cellular phones. Several variants for the same solution were proposed and all of the implementations use third-party products such as radios (motes) and sensor interfaces [11]. The motes are battery-powered devices that run specific software. These motes are ready-to-use wireless modules, where boards with sensors are attached. Their primary advantage rapidly fades and turns into a severe drawback, because the primary goal is to have wireless platforms integrating the industrial environment. Thus, more compact and low-sized modules are needed. Also, these solutions are too much expensive for high-mass production and thus, for industrial use. The integration of RF transceivers with dimensions comparable to the other Microsystems elements permit the fabrication of even more compact, low-size and low-power modules, supplied by a single battery. Miniaturized Microsystems contribute to the mass production with low prices, favoring the spread of applications for these Microsystems. Moreover, solutions relying on wireless Microsystems offer the flexibility of including as many modules as required and selecting any type of sensors to be assembled with the RF transceiver and the other electronics. The CMOS-WiI has low power, low voltage, and it allows the independent activation of each subsystem. In terms of project and design, it is straightforward to provide the power supply of all the system-blocks integrated in the same Microsystems since the feeding points are reduced and the battery coupling is more effective.

The CMOS-WiI can be used to connect the wireless modules to the EEG electrodes on the individual's scalp and transmit the acquired data to a portable device. This device forwards the acquired data to a base station (e.g., the central processing unit), which stores and does the signal processing. Fig. 4 shows the system architecture of the CMOS-WiI to mount a wireless sensors network with wireless modules comprised of dry EEG electrodes and the CMOS-WiI. A set of 16 different frequencies (with a spacing of 27.12 MHz) were conceived, in order to make possible the existence of multiple transmissions (independently of their relative priority) between the different wireless modules placed in the patient's head. The wireless communication is not between the wireless modules, but also between these and with a base station that stores the acquired data for further
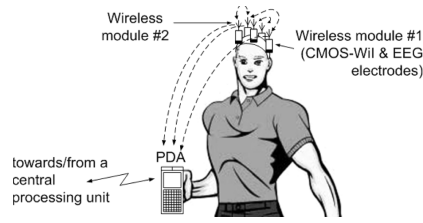
Fig. 4. System architecture of the CMOS WiI.

Fig. 5. Block schematic of the transceiver.

processing. The easy mounting/removing of wireless modules to/from where desired, is another advantage.

III. RF CMOS Transceiver Design

A. Selection of the Frequency Band

The frequency selection for the CMOS-WiIs took into account the need to obtain compact and miniaturized solutions. Moreover, the possibility to include chip-size antennas in the RF microsystem was a crucial (and mandatory) requirement to comply with the former goal. In order to implement efficient power-consumption wireless sensor networks, it was also necessary to develop a low-power/low-voltage RF CMOS transceiver, suitable for mounting in the antenna. In wireless communications, the antenna is one of the most critical subsystem, thus, in order to not compromise the desired miniaturization, the antenna must be small enough to comply with size constraints of the microsystems. The investigation of new frequency bands [12] and new geometries [13] allow the development of smaller antennas to integrate in wireless microsystems [14], [15]. Also, the dimension of an antenna is proportional to the operating wavelength. Thus, the migration of wireless communication systems to higher frequency bands (as is the case of the 5–6 GHz ISM band) facilitates on-chip implementation of antennas [12]. This makes the frequency selection one of the more decisive tasks, when RF transceivers are designed. Normally, the frequency must take some key features into account: the desired range, the baud rate and the power consumption. However, these features trade between them. The attenuation of RF signals in the free-space increases with the distance, thus for a simultaneously given transmitted power, P_t [dB], and receiver's sensitivity, S_r [dB], the frequency of operation is limited by the range, d_{max} [m], e.g., $f \leq 10^{[(P_t - S_r) - 20\log_{10}(4\pi d_{max})]/20}$ [Hz] [13]. It must be noted that an increase in the power of RF signals, P_t [dB] compensates for the additional losses in the radiowave channel. However, an increase in the transmitted power implies a higher power consumption, which results in a shorter battery life. Therefore, increasing the transmitted power is an unacceptable solution, especially when the goal is to keep or even increase the battery life. Applications that need high baud rates also require high signal bandwidths. However, the operating frequency cannot be arbitrarily increased, because this will have implications in the power consumptions, e.g., at high frequencies, the transistors must switch faster, thus the energy dissipation will be higher. Finally and not less important, the output power and the distance also trade with the noise, N [dB], in the receiver
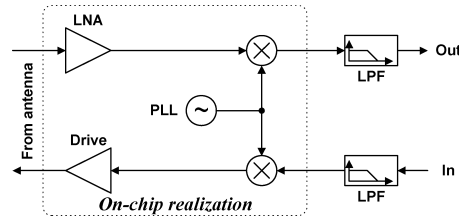
site, thus with the bit error probability (BEP). The BEP for ASK systems with envelope detection is $1/2 \cdot \exp(-(1/2)\gamma_0)$, $\gamma_0 \gg 1$ [16], where γ_0 is the signal-to-noise ratio (SNR) at the receiver site. The equation for the BEP imposes the need to have a minimum SNR in the receiver site. This means that a maximum BEP of 10^{-6} (which is acceptable in the acquiring of EEG signals) implies $\gamma_0 \geq 26$ (or $\gamma_{0\,dB} \geq 14$ dB). Finally, the minimum power, P_R [dB] (or p_r [W]), of RF signals in the RF receiver is such that $\gamma_{0\,dB} \geq P_R - N$ dB (N [dB] is the noise power in the receiver site) thus, the sensitivity of the RF receiver must be at least equal to $\gamma_{0\,dB} + N$. The best free-usage frequencies for wireless devices are those belonging to the so-called Industrial, Scientific and Medical (ISM) band, due to its unregulated usage. This means that these frequencies are not subjected to standardization and can be freely used, since the emission powers are kept below the maximum levels imposed by national legislation. This usage flexibility lead to the rise and widespread of new and interesting applications. All of these and the former system-implementing features were decisive during the selection of CMOS-WiI operating frequency, whose value was selected to be around the 5.7 GHz.

B. Architecture of the RF CMOS Transceiver at 5.7 GHz

The 0.18 μm RF CMOS process from United Microelectronics Corporation (UMC) was used for the fabrication of a 5.7-GHz RF CMOS transceiver. This process has a polysilicon layer and six metal layers, allowing integrated spiral inductors (with a reasonable quality factor, e.g., in the range 4–10), high resistor values (a special layer is available) and a low-power supply of 1.5 V. Therefore, high on-chip integration is possible, in favor of better repeatability as well as lower pin count [17]. An important issue to take into account during the project of RF transceivers for use in any wireless network is that without proper design, the communication tasks may increase network power consumption significantly because listening and emitting are power-intensive activities [18]. Thus, the power consumption of a RF transceiver can be optimized by predicting in the design the possibility to use control signals. The functions of such signals are to enable and disable all subsystems of the RF transceiver. These signals allow the switch-off of the receiver when a RF signal is being transmitted, to switch-off the transmitter when a RF signal is being received, and allows the RF transceiver to enter sleep mode when RF signals are neither being transmitted nor received. Fig. 5 shows the RF CMOS transceiver architecture, which is composed by a receiver, a transmitter, and a frequency synthesizer. The receiver adopts a direct demodulation, by means of envelope detection. The RF CMOS transceiver
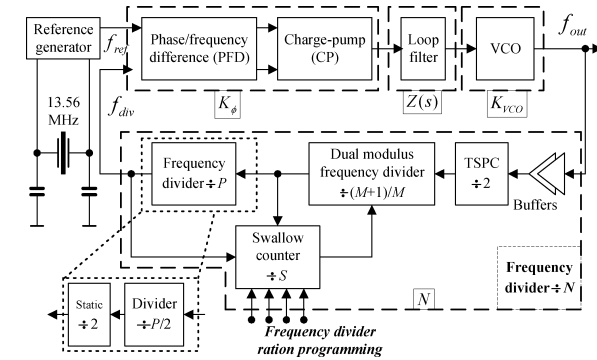

Fig. 6. Block diagram of the PLL.

is constituted by a low-noise amplifier (LNA) that provides an input impedance of 50 Ω, the amplified RF signal is directly converted to the baseband with a single balanced active MOS mixer. The internal oscillator at 5.7 GHz is a phase-locked loop (PLL).

The RF CMOS transceiver can operate in the frequency range of 5.42–5.83 GHz. This is done by changing the frequency division ratio in the feedback path of the PLL. The PLL has four digital inputs to select one in 16 possible division ratios. The output frequency is given by $f_{out} = f_{ref} \times 2 \times (200 + D)$, where D is the equivalent decimal of digital inputs for a reference frequency of $f_{ref} = 13.56$ MHz. The lowest noise-figure (NF) of the LNA is achieved with an inductively degenerated common source amplifier with tuned load. In these conditions, the input impedance at 5.7 GHz for matching with the antenna is easily adjusted to 50 Ω. The cascode architecture is the one that allows the higher isolation between the output and the input, but is not suitable for low supply voltage applications [19]. Thus, a single-transistor topology was selected for the LNA. Also, because the LNA has a single transistor in the amplifier, a sacrifice in the gain was observed, but the NF also decreased. Fig. 6 does not show the circuits to bias the LNA. The up-conversion and the down-conversion operations are done with two mixers that are ac-coupled to the LNA and are modified versions of the Gilbert cell [20]. Also, both mixers are directly driven by the differential outputs of the on-chip frequency synthesizer. The drive circuit acts a buffer between the up-conversion and an external power amplifier (PA). For a complete on-chip solution, this drive circuit can be used, but with a smaller range. However, this is not a problem for the proposed network because the distances are small (limited to the dimensions of the patient's head).

C. Frequency Synthesizer (PLL)

An on-chip frequency synthesizer provides local versions of the carrier frequencies to both the down-conversion and the up-conversion mixer. This frequency synthesizer is a PLL with an integer divider in the feedback loop, whose dividing ratio can be digitally programmed to generate local carrier frequencies in the 5.42–5.83 GHz frequency range.

Fig. 6 illustrates a block diagram showing the structure of the PLL. This PLL has a reference generator circuit with a crystal-based oscillator at 13.56 MHz, followed by a phase-frequency difference circuit (PFD), a current steering charge pump (CP), and a third-order passive filter. The passive section output is connected to the VCO, that generates the desired frequency range of 5.424–5.830 GHz. Finally, in order to get the desired frequency in the previous range, this one must be divided by $400 + 2S$, where S is integer and belongs to the interval $\{0, 1, \ldots 15\}$. Then, the output of the divider is connected to the PFD, closing the loop. The output frequency produced by the PLL depends on the divider ratio, N, and is $f_{out} = f_{ref} \cdot N$ [Hs]. The PLL acts a frequency multiplier of the reference frequency, f_{ref} [Hz].

The desired divider ratio, N, in the feedback path can be selected in the following way: $N = 2(M \cdot P + S)$. The two values $(M + 1)$ and M (with $M = 10$) are the variable frequency divider ratios in the prescaler, $S = 20$ is the divider ratio in the main counter, and S is the divider ratio in the swallow counter. The main counter has a circuit to divide by $P/2 = 10$ followed by a toggle flip-flop, to make the feedback signal at the divided input of the PFD, f_{div}, to present a duty-cycle of 50% (as happens with the reference signal at the main input, f_{ref}, of the PFD). Input signals in the PFD with duty-cycles of 50% minimize possible delays that can arise, during the locking process of the PLL.

IV. Dry Electrodes Fabrication

A wet-etch process using KOH was applied in the micro-fabrication of the silicon micro-tips. The tip shape was defined by the undercut effect in the etch process, where locally fastest-etching planes are revealed. A silicon wafer with $\langle 100 \rangle$ orientation was used with a silicon nitride layer as a mask for the etching. The micro-fabrication process of the micro-tips is illustrated in Fig. 7.

In the first step, a mask with 200 μm square features was used on the lithography process for micro-tip definition. The chosen size for the mask features came as a result of previous analysis of the mask characteristics effect. The 200 μm offered not only a locked aspect ratio in terms of print resolution, but also provided
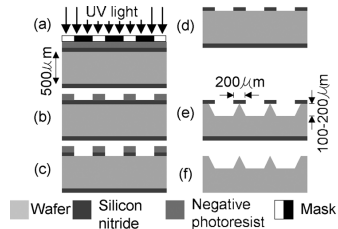
Fig. 7. Schematic of the six steps employed on the micro-tip structures fabrication.
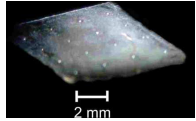

Fig. 8. Optic microscope image of a micro-tips array.

better control of the etching progression, since more time was needed for the tip formation. In the second step, the photoresist was removed from the areas that were not covered by the photomask. Then, the silicon nitride layer opened windows allowed exposition to its elimination in the third step. The remaining areas with silicon nitride worked out as a protection layer for the Si wafer's etching process with a 30% KOH solution at a temperature of $87\,^\circ$C, ensuring a etch rate of $1.6\,\mu\mathrm{m}/\min$. Finally, a conductive layer of IrO was deposited on the surface of an array of stable micro-tips electrodes to guarantee the ability to overcome the insulation skin layer (e.g., the *stratum corneum*) and, thus, minimize the resistivity of the interface electrode/skin. The thin-film resistance was measured through the *van der Pauw* method since it is a crucial issue for biopotential electrodes. The lowest resistance value along all sputtering sessions was $166.49 \times 10^{-7}\,\Omega \cdot \mathrm{cm}$ in a 2-$\mu\mathrm{m}$ thick film.

The micro-machined tips with an IrO thin film resulted in a three-dimensional (3-D) structure capable of bypassing the skin nonconductive layer with a low-resistance IrO film on its surface and enabling excellent biopotential recording functions (see Fig. 8).

V. CMOS-WiI MODULE

The CMOS-WiI is composed by a sensor interface, to provide protection against electrostatic discharge (ESD). It also comprises the electronics for processing and control, the memory, a RF CMOS transceiver, and a pair of PADs to provide connections to an associated antenna. All of these components are integrated in the same microsystem by use of multi-chip-module (MCM) techniques. The block diagram of the CMOS-WiI (shown in Fig. 9) permits its usage as a plug-and-play module for EEG caps. In order to simplify the physical mounting of a wireless sensors networks, the identification protocols allow the placement and removal of the modules, according the medical doctor's need. This brings a new concept in wireless sensors networks and in EEG networks, e.g., the plug-and-play concept.
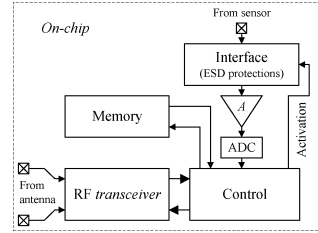

Fig. 9. Block diagram of microsystems to mount a wireless sensors network in the head of an individual.

As the data is periodically acquired in all of the modules, the latencies of data transmissions are not allowed. The CMOS-WiI uses a communication protocol that overcomes these problems [21]. The protocol combines the distributed and coordination modes, e.g., when a new module is placed, a contention-based time interval is used to make the registration request in the network. A contentionless time interval, constituted by time-slots, is granted to the new module if the registration is successfully completed on the network. The maximum number of simultaneous modules is limited to the number of time-slots in the contention-free interval. A network coordinator periodically generates a beacon, to make frame synchronization in order to let the different nodes know when they start the time-slot for which access to the medium was granted. The Manchester coding was used in the symbol synchronization for ASK transmission, e.g., for each databit to be sent, a set of two Manchester symbols are transmitted at twice the bitrate. More precisely, if a "1" or a "0" is to be sent, then, the Manchester sequence "10" or "01" is transmitted during the duration of a bit. Moreover, this is especially useful in the presence of long data sequences of "1s" or "0s". This communication protocol ensures that the conceptual separation between the sensing and the information, communication, and entertainment subsystems is obtained and their coexistence is achieved. Also, the power selection feature offered by the RF transmitter, makes it possible to include a power-efficient variant in this protocol.

VI. RESULTS

A. RF CMOS Transceiver

For frequencies in the range 5.420–5.830 GHz, the LNA has a gain in the range 9.60–9.81 dB, a stabilization factor K of 1.21, making the LNA unconditionally stable ($K > 1$). Also, the noise figure, NF [dB], of the LNA is in the range 2.78–2.84 dB. The graph in Fig. 10 is the linearity analysis of the LNA, which reveals a third-order intercept point, IP3, of 9.1 dBm.

The VCO has a constant $K_{\mathrm{VCO}} \approx 2.8$ [GHz/V], obtained from the linear range of the voltage-to-frequency (V/F) characteristic. The charge-pump has *up* and *down* currents of 269 μA and 201 μA, respectively, and a detector gain constant $K_\phi = 75\ \mu\mathrm{A}/2\pi$ rad. The *up* and *down* currents of 269 μA and 201 μA, respectively, and a detector gain constant $K_\phi = 75\ \mu\mathrm{A}/2\pi$ rad. The power consumptions are about 9.65 mW for the LNA, 9.51 mW for the mixers, and 4.14 mW
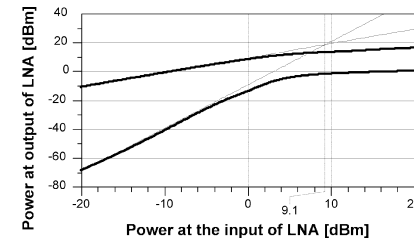
Fig. 10. The 3-dB intercept point (IP3) of the LNA.

TABLE I
THE COMPARISON OF THE RF CMOS TRANSCEIVER WITH OTHER FOUND ON THE RELATED STATE-OF-THE-ART

RF band [GHZ]	Power consumpsion [mW]	Power supply [V]	Remarks	Ref
5.42-5.83	9.65	1.5	LNA	This work
	9.51		Mixers	
	4.14		PLL	
5.25	114	3	Receiver	[22]
5.70	120		Transmitter	
5.15-5.35	250	3.3	Receiver	[23]
	790		Transmitter	
5.15-5.35	12.4	2	Receiver	[24]
5.15-5.35	320	1.8	Receiver	[25]
	260		Transmitter	

for the PLL. Table I compare this RF CMOS transceiver with others found on the related state-of-the art.

B. Electrodes

A set of experiments were done in order to assess the electrochemical characteristics of the dry electrodes as well as their interface with the electrolyte. In Fig. 11(a) and (b), the conductivity and relative permittivity were plotted, respectively, for the whole frequency range 1–1000 Hz. The sample standard deviation is represented by a vertical bar for each measured frequency. In electrochemical analyses, the admittance values are often assessed instead of the impedance values actually read. It should be noted that the admittance ($Y = G + \mathrm{j}B$, G is conductance, B is susceptance) is the reverse of the impedance values (impedance $Z = R + \mathrm{j}X$, R is resistance, X is reactance). The conductivity is the cell-geometry-independent value of the conductance (G) and usually assumed as the reverse of the resistivity (i.e., material property that is the cell-geometry-independent value of the resistance). The conductivity ranges from around $5\ \mathrm{mS}\cdot\mathrm{cm}^{-1}$ for 1 Hz to almost $14\ \mathrm{mS}\cdot\mathrm{cm}^{-1}$ for 1000 Hz. The IrO electrodes show a conductivity that is significantly different from the AgCl electrode for frequencies below 3 Hz. Both electrode types exhibit comparable conductivity for frequencies above 3 Hz. Relative permittivity (ε_r) is the cell-geometry-independent value of the susceptance (B) with respect to vacuum permittivity (ε_0 is $8.8\mathrm{e}10^{-14}\ \mathrm{F}\cdot\mathrm{cm}^{-1}$) and gives some insight about the amount of capacitive behavior of each electrode type. The AgCl electrodes relative permittivity ranges from 3.5×10^5 for 1000 Hz to 10^{10} for 1 Hz. The IrO electrodes relative permittivity is slightly higher than AgCl electrodes' for frequencies
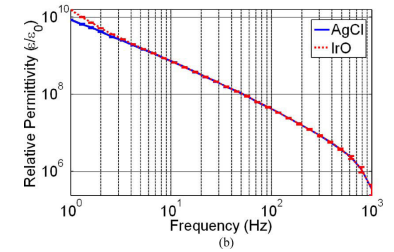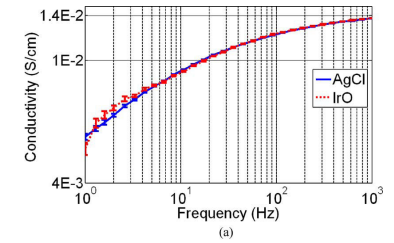

Fig. 11. (a) Conductivity (σ) of the fabricated electrodes (red dashed line) and of the control Ag/AgCl electrodes (blue solid line), for the whole frequency range (1–1000 Hz). (b) Relative permittivity (ε_R) of the fabricated IrO electrodes (red dashed line) and of the control Ag/AgCl electrodes (blue solid line), for the whole frequency range (1–1000 Hz).
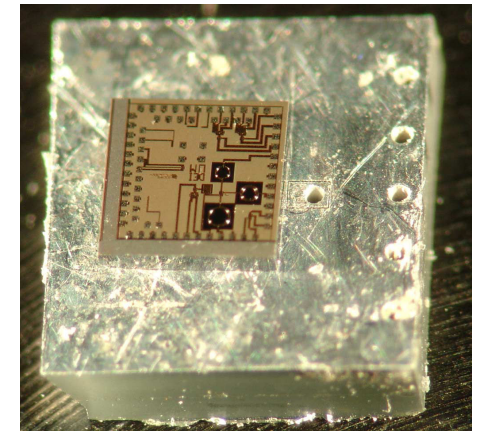

Fig. 12. Module photograph, where the electronics (the CMOS-WiI microchip) is ready to be mounted with a chip-size planar antenna with an area of $3.6 \times 3.6\,\mathrm{mm}^2$.

below 3 Hz. The higher permittivity is exhibited by IrO electrodes for frequencies below 3 Hz, in addition to a more negative impedance phase, mean that the IrO electrodes are more capacitive than AgCl electrodes for low frequencies. For frequencies
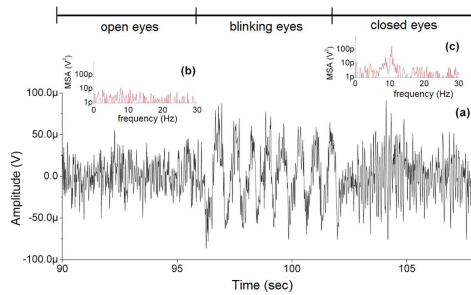
Fig. 13. Acquired EEG signal with a sampling frequency of 100 Hz, a pass-band in the range 1–30 Hz, and with the individual doing three tasks: (a) with the eyes opened, (b) with the eyes blinking, and (c) with the eyes closed.

above 3 Hz, both electrodes show comparable behavior in conductivity, permittivity, and phase plots. Therefore, no electrode shows best performance over the entire frequency range.

The error bars in Fig. 11 were obtained from repeated measurements. For a set of N measurements, $x_i, i \in \{1, 2, \ldots, N\}$, the center and the half-length of the respective lines is equal to medium value and to standard deviation. The medium and the standard deviation are given by $\overline{X} = (\sum_{i=1}^{N} x_i)/N$ and $\sigma = \sqrt{\sum_{i=1}^{N}(x_i - \overline{X})^2/N}$.

C. CMOS-WiI Module

Fig. 12 is a photograph of a full wireless module, where it is shown that the CMOS-WiI measuring of $1.5 \times 1.5 \ \mathrm{mm}^2$ ready to be mounted with a chip-size planar antenna with an area of $3.6 \times 3.6 \ \mathrm{mm}^2$. Experiments were conducted while a subject was performing three different tasks: eyes opened, blinking, and eyes closed. Fig. 13 shows an EEG signal acquired with these IrO electrodes for this subject. This signal was acquired with a individual doing a set of three tasks. These tasks consisted of the individual holding the eyes opened; blinking the eyes, and keeping the eyes closed.

VII. CONCLUSIONS

The CMOS-WiI presents a total power consumption of 23 mW. These characteristics fulfill the requirements for short-range communications for using the 5.7-GHz ISM band. The target application of CMOS-WiI is to provide intrawireless module communication. Table II allows the comparison of CMOS-WiI with other state-of-the-art solutions. Two types of solutions were analyzed, e.g., customized and commercial of-the-shelf (COTS) solutions. The dry IrO electrodes with microtips for biopotential recordings were intended to avoid skin preparation (i.e., electrolyte application and skin abrasion). The conductivity values suggested that the resistive behaviors of both recording materials (Ag/AgCl and IrO) are comparable for the whole frequency range. The unequal behavior of the IrO and Ag/AgCl materials, for frequencies below 3 Hz, seems to be due to different kinds of charge transmission. A 3-D structure (microtip) capable of bypassing the skin nonconductive layer, with a low-resistance IrO film on its surface, permits the

TABLE II
COMPARISON OF CMOS-WiI WITH OTHER BEST RELATED STATE-OF-THE-ART WIRELESS SOLUTIONS

	CMOS-WiI	Tokyo [26]	UCLA [27]	Duke [28]
Type	Customized	Customized	COTS	COTS
# channels	16	1	6	12
Resolution	16 bits	Analog: not applicable	8 bits	12 bits
Baud-rate [kbps]	up to 250	Analog: not applicable	9.6	Not available
Range [m]	10	16	2	9
Modulation & coding	ASK & Manchester	Analog FM	FSK	802.11b
Carrier frequency	5.7 GHz	Not available	800/900MHz	2.4 GHz
MAC protocol	Hybrid TDMA & CSMA-CA	Not available	Not available	Not available
RF system consumption	23 mW	10 mW	66 mW	333 mW
Supply [V]	1.5	3	3	3.3-5
Type of acquisition	Not invasive	Invasive	Invasive	Invasive

construction of a biopotential recording/stimulating electrode with fast application. In conclusion, the application of dry IrO electrodes in the CMOS-WiI to mount a wireless sensors network in the subjects's head to record EEG signals allows them to maintain their mobility while simultaneously having their electrical brain activity monitored. Thus, this solution provides a breakthrough in the monitoring, diagnostics, and treatment of patients with neural diseases, such as epilepsy [1].

REFERENCES

[1] "IMEC press releases, 'Ambulatory EEG'," in *Human ++ EU Project*. Leuven, Belgium: IMEC, 2003, pp. 1–2.

[2] M. R. Werner and W. R. Fahrner, "Review on materials, microsensors, systems and devices for high-temperature and harsh-environment applications," *IEEE Trans. Ind. Electron.*, vol. 48, no. 4, pp. 249–257, Apr. 2001.

[3] W. R. Patterson *et al.*, "A microelectrode/microelectronic hybrid device for brain implantable neuroprosthesis applications," *IEEE Trans. Biomed. Eng.*, vol. 51, no. 10, pp. 1845–1853, Oct. 2004.

[4] S. Grimnes and Ø. G. Martinsen, *Bioimpedance and Bioelectricity Basics*. London, U.K.: Academic, 2000.

[5] J. Griss *et al.*, "Characterization of micromachined spiked biopotential electrodes," *IEEE Trans. Biomed. Eng.*, vol. 49, no. 6, pp. 597–604, Jun. 2002.

[6] T. C. Ferree *et al.*, "Scalp electrode impedance, infection risk and EEG data quality," *Clin. Neurophysiol.*, vol. 112, pp. 536–544, 2001.

[7] W. Mokwa, "MEMS technologies for epiretinal stimulation of the retina," *J. Micromech. Microeng.*, vol. 14, no. 9, pp. S12–S16, 2004.

[8] P. Johansson *et al.*, "Bluetooth: An enabler for personal area networking," *ACM/IEEE Trans. Netw.*, vol. 15, no. 5, pp. 28–37, May 2001.

[9] V. C. Gungor and G. P. Hancke, "Industrial wireless sensor networks: Challenges, design principles, and technical approaches," *IEEE Trans. Ind. Electron.*, vol. 56, no. 10, pp. 4258–4265, Oct. 2009.

[10] K. A. Agha *et al.*, "Which wireless technology for industrial wireless sensor networks? The development of OCARI technology," *IEEE Trans. Ind. Electron.*, vol. 56, no. 10, pp. 4266–4278, Oct. 2009.

[11] J. Hill *et al.*, "System architecture directions for networked sensors," in *Proc. Architectural Support for Programming Languages and Operating Systems*, 2000, pp. 93–104.

[12] P. M. Mendes *et al.*, "Integrated chip-size antennas for wireless microsystems: Fabrication and design considerations," *J. Sens. Actuators A*, vol. 125, pp. 217–222, Jan. 2006.

[13] P. M. Mendes *et al.*, "Analysis of chip-size antennas on lossy substrates for short-range wireless microsystems," in *Proc. SAFE 2002*, Nov. 27–28, 2002, pp. 51–54.

[14] J. A. Gutierrez *et al.*, "IEEE 802.15.4: A developing standard for low-power low-cost wireless personal area networks," *IEEE Netw.*, vol. 15, no. 5, pp. 12–19, Sep. 2001.

[15] C. C. Enz et al., "Ultra low-power radio design for wireless sensor networks," presented at the IEEE Int. Workshop Radio-Frequency Integration Technology: Integrated Circuits for Wideband Communication and Wireless Sensor Networks, Singapore, Dec. 2005.

[16] B. Carlson et al., *Communication Systems – An Introduction to Signals and Noise in Electrical Communications*4th ed. New York: Mc-Graw-Hill, 2001.

[17] P. Choi et al., "An experimental coin-sized radio for extremely low-power WPAN (IEEE 802.15.4. applications at 2.4 GHz," IEEE J. Solid State Circ., vol. 8, no. 12, pp. 2258–2268, Dec. 2003.

[18] C. C. Enz et al., "WiseNET: An ultra low-power wireless sensor network solution," IEEE Comput. , vol. 37, no. 8, pp. 62–67, Aug. 2004.

[19] C.-P. Chang et al., "A 1-V, 6-mA, 3–6 GHz broadband 0.18- μm CMOS low-noise amplifier for UWB receiver," Microw. Optical Technol. Lett., vol. 49, no. 6, pp. 1358–1360, Mar. 2007.

[20] G. Gramegna et al., "A 35-mW 3.6- mm^2 fully integrated 0.18μm CMOS GPS radio," IEEE J. Solid State Circ. , vol. 39, no. 7, pp. 1163–1171, Jul. 2004.

[21] J. Afonso et al., "MAC protocol for low-power real-time wireless sensing and actuation," inProc. 13th IEEE Int. Conf. Electronics, Circuits and Systems, Nice, France, Dec. 2006, pp. 1248–1251.

[22] L. T.-P. Liu and E. Westerwick, "5-GHz CMOS radio transceiver front-end chipset," IEEE J. Solid-Stace Circ. , vol. 35, no. 12, pp. 1927–1933, Dec. 2000.

[23] M. Zargari et al., "A 5-GHz CMOS transceiver for IEEE 802.11a wireless LAN systems," IEEE J. Solid-Stace Circ. , vol. 37, no. 12, pp. 1688–1694, Dec. 2002.

[24] H. Samavati et al., "A 5-GHz CMOS wireless LAN receiver front end," IEEE J. Solid-Stace Circ. , vol. 37, no. 5, pp. 765–772, May 2004.

[25] K. Vavelidis et al., "A dual-band 5.15–5.35-GHz, 2.4–2.5-GHz 0.18-μm CMOS transceiver for 802.11a/b/g wireless LAN," IEEE J. Solid-Stace Circ., vol. 39, no. 7, pp. 1180–1184, Jul. 2004.

[26] S. Takeuchi and I. Shimoyama, "A radio-telemetry system with a shape memory alloy microelectrode for neural recording off reely moving insects," IEEE Trans. Biomed. Eng. , vol. 51, no. 1, pp. 133–137, Jan. 2004.

[27] S. Farshchi et al., "A TinyOS-enabled MICA2-based wireless neural interface," IEEE Trans. Biomed. Eng. , vol. 53, no. 6, pp. 1416–1424, Jun. 2006.

[28] I. Obeid et al., "A multichannel telemetry system for single unit neural recordings," J. Neurosci. Meth., vol. 133, pp. 33–38, 2004.
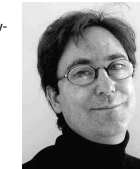
Dr. Dias is also a Member of the IEEE Industrial Electronics Society, and of the IEEE Engineering in Medicine and Biology Society.

João Paulo Carmo (S'02–M'08) was born in 1970 in Maia, Portugal. He received the B.S. and M.Sc. degrees in electrical engineering from the University of Porto, Porto, Portugal, in 1993 and 2002, respectively. In 2007, he received the Ph.D. degree in industrial electronics from the University of Minho, Guimarães, Portugal. His Ph.D. thesis was on RF transceivers for integration in microsystems to be used in wireless sensors network applications.
Since 2008, he is an Assistant Researcher at the Algoritmi Center, University of Minho. He is involved in the research on micro/nanofabrication technologies for mixed-mode/RF systems, solid state integrated sensors, and microactuators and micro/nanodevices for use in wireless and biomedical applications.
Dr. Carmo is also a Member of the IEEE Industrial Electronics Society.

Paulo Mateus Mendes (M'05) received the B.S. and M.Sc. degrees in electrical engineering from the University of Coimbra, Coimbra, Portugal, in 1995 and 1999, respectively. He obtained his Ph.D. degree in industrial electronics from the University of Minho, in 2005.
Since 2006, he has been an Assistant Professor at the University of Minho, and a Researcher at the Algoritmi Center there. He has been involved in several projects related to project, fabrication, and characterization of microantennas for wireless microsystems.
Dr. Mendes is Member of the European Microwave Association, of the IEEE Antennas and Propagation Society, and of the IEEE Engineering in Medicine and Biology Society.

Nuno Sérgio Dias (M'09) received the B.S. degree in industrial electronics and computers from the University of Minho, Guimarães, Portugal in 2004. In 2009, he received the Ph.D. degree in industrial electronics from the University of Minho, in collaboration with the Center for Neural Engineering at The Pennsylvania State University, State College. His Ph.D. degree thesis was on brain-machine interface based on biotelemetry and dry electrodes.
He is currently a Post-Doc Researcher with the Life and Health Sciences Research Institute – ICVS, University of Minho, Braga, Portugal.

José Higino Correia (S'96–M'00) received the B.S. degree in physical engineering from University of Coimbra, Coimbra, Portugal, in 1990. He received the in 1999 a Ph.D. degree fom the Laboratory for Electronic Instrumentation, Delft University of Technology, Delft, The Netherlands, in the field of microsystems for optical spectral analysis in 1999.
He is currently a Full Professor in Department of Industrial Electronics, University of Minho, Portugal.
His professional interests are in micromachining and microfabrication technology for mixed-mode systems, solid-state integrated sensors, microactuators and microsystems. Professor Correia is also a Member of the IEEE Industrial Electronics Society. He was the General-Chairman of Eurosensors 2003 and MME 2007, Guimarães, Portugal.